Available online at www.sciencedirect.com

ScienceDirect

Materials Today: Proceedings 5 (2018) 10431–10439

materialstoday: PROCEEDINGS

www.materialstoday.com/proceedings

AEMC_2017

Incorporation of UiO-66 into Graphene Foam for Hydrogen Storage Applications

Sonwabo E. Bambalaza[a,b], Henrietta W. Langmi[a]*, Nicholas M. Musyoka[a], Jianwei Ren[a], Lindiwe E. Khotseng[b]

[a]*HySA Infrastructure Centre of Competence, Materials Science and Manufacturing, Council for Scientific and Industrial Research (CSIR), PO Box 395, Pretoria 0001, South Africa*

[b]*Faculty of Natural Science, University of the Western Cape, Bellville, Cape Town 7535, South Africa*

Abstract

The fabrication of application-specific metal-organic framework (MOF) composites has the potential to shift more towards hydrogen storage system integration. The *in-situ* growth of nano particles on a graphene surface is a common technique for synthesizing graphene-inorganic nanocomposites and in this study, a graphene foam (GF) / zirconium-based MOF (UiO-66) composite was prepared using a two-step solvothermal method. Brunauer, Emmett and Teller (BET) surface area as well as hydrogen uptake capacity were measured under cryogenic conditions and compared to the values for pristine UiO-66. The GF/UiO-66 composite had a BET surface area of 1073 $m^2.g^{-1}$ and a hydrogen uptake capacity of 1.1 wt% at 77 K and 1.2 bar pressure, compared to 1367 $m^2.g^{-1}$ and 1.5 wt%, respectively for pristine UiO-66 under the same conditions. Besides the values being compromised relative to pristine UiO-66, the two-step *in-situ* synthesis approach yielded a composite with enhanced BET surface area and H_2 uptake relative to a composite obtained from a single step synthesis approach. The composites further exhibited better thermal stability than the pristine UiO-66 and show promise for the development of powdered MOF materials towards hydrogen storage system integration.

Selection and/or Peer-review under responsibility of 1st Africa Energy Materials Conference.

Keywords: Graphene foam; UiO-66; Hydrogen uptake; Zr-MOF

* Corresponding author. Tel.: +27 128412604; fax: +27 8412135.
E-mail address: hlangmi@csir.co.za

Selection and/or Peer-review under responsibility of 1st Africa Energy Materials Conference.

1. Introduction

Metal-organic frameworks (MOFs) are highly crystalline nano-scale compounds consisting of a metal center and hydrocarbon linker molecules. The chemical bonding in MOFs gives rise to crystal structures with permanent porosity, with the size of the pores typically determined by the length of the hydrocarbon linker. Generally, MOFs exhibit high surface areas, with an experimental value of up to 7140 $m^2.g^{-1}$ reported [1], and high pore volumes. These properties make MOFs ideal for their application in gas storage by physisorption. The synthesis methods for MOFs are relatively simple, such as solvothermal, microwave-assisted and solvent-free synthesis, and can be scaled-up easily. Additionally, MOFs textural properties can be tailored by altering their synthesis parameters or starting feedstock materials [2-4]. It is therefore, highly feasible to tailor their application-specific properties in order to integrate them into high performance gas storage technologies/systems.

One of the ongoing research topics on MOFs is their use to store molecular hydrogen gas (H_2) for applications in fuel-cell vehicles and other fuel-cell based technologies [5-7]. Our research has focused on the synthesis, up-scaling, and system integration of chromium- and zirconium-based MOFs for their application as H_2 storage materials. As previously reported [8], the Cr-MOF and Zr-MOF were obtained as loose powders which are difficult to handle. It has also been shown that some MOFs, such as MOF-5, in powder form have relatively low packing density and thermal conductivity [9]. In order to address this challenge, some densification methods such as pelletisation and granulation have been shown to improve the packing density of the MOFs [8,9]. The risk, however, is that with these methods the maximum gravimetric H_2 uptake capacities become compromised. The decreased H_2 uptake can be attributed to either the partial MOF amorphisation that can occur during densification or the interferences of the binders used during granulation, which are typically non-porous or do not contain micropores suitable for H_2 adsorption [8,9]. In order to overcome some of the challenges of working with pristine powdered MOF materials, alternative approaches such as generating composites of MOFs with other compounds that can potentially improve some of the MOF properties without substantially compromising H_2 uptake capacities, are needed for system integration.

In this study, we focus on the synthesis of Zr-MOF/graphene foam composites. Graphene in itself is considered a hydrogen storage material [10]. Graphene also has good thermal conductivity and hence can readily dissipate heat build-up when exposed to high-pressure gas [11-13]. This work employed an *in-situ* method to incorporate the Zr-MOF, UiO-66, into graphene foam (GF). The approach aims to derive possible synergistic effects that may arise from compositing UiO-66 with GF with regards to properties suitable for a hydrogen storage medium. A two-step *in-situ* synthesis method was used in order to incorporate more UiO-66 into GF.

2. Materials and methods

2.1. Reagents and chemicals

Zirconium tetrachloride ($ZrCl_4$, Sigma Aldrich, 99.5+%), terephthalic acid (Sigma Aldrich, 98%), N,N-dimethylformamide (DMF, Sigma Aldrich, 99.8%), formic acid (HCOOH, Sigma Aldrich, 95+%), and hydrochloric acid (HCl, Sigma Aldrich, 36.8 – 38%) were purchased and used without further purification. Ni foam (Celmet, Japan: thickness = 1.6 mm, surface area = 7500 $m^2.m^{-3}$, cell size = 0.5 mm, 48-52 cells per inch) was used with no further treatment. Deionized water was obtained from a water purification system (Barnstead Smart2Pure, Thermo Scientific) in our laboratory.

2.2. Preparation of UiO-66 crystals

The modulated synthesis approach for UiO-66 crystals was based on a previously reported method [14] with minor changes. In a typical procedure, 0.22 mol $ZrCl_4$ and 0.22 mol terephthalic acid were mixed in 50 mL DMF in a 100 mL Teflon cylinder and subjected to ultrasonication for 30 minutes. A 100 mol equivalent (relative to $ZrCl_4$) of formic acid was then added to the mixture and left to stand for 60 s.

The mixture was transferred to a steel bomb reactor and kept for 8 h at 120 ^{o}C in a pre-heated oven. After the synthesis, the product was washed three times in DMF to remove unreacted terephthalic acid by centrifuging at 10000 rpm for 10 minutes. The crystals were then dried under vacuum at 90 ^{o}C for 24 h.

2.3. *Preparation of GF*

Graphene foam was prepared using the chemical vapor deposition (CVD) technique [15-18]. In a typical procedure (also shown in Fig. 1), a 20 mm x 20 mm x 1.6 mm Ni foam sample was placed on an alumina crucible and heated to 800 ^{o}C at 5 ^{o}C.min^{-1} under an Ar flow (0.5 dm^{3}.min^{-1}). This was followed by isothermal annealing for 20 min under Ar/H_2 (0.5 dm^{3}min^{-1} / 0.025 dm^{3}.min^{-1}) to clean the Ni foam surface of any impurities, and then ramping to 1000 ^{o}C at 5 ^{o}C.min^{-1} under the same conditions. At 1000 ^{o}C, acetylene gas (C_2H_2) (0.025 dm^{3}.min^{-1}) was introduced as a carbon precursor and the reaction was carried out for 15 min. After the reaction, the sample was cooled gradually to 200 ^{o}C followed by rapid cooling to room temperature. Prior to removing the Ni template, the sample was first coated with a 50 mg.mL^{-1} solution (in acetone) of polymethylmethacrylate (PMMA) in order to maintain structural integrity of GF during the etching process. The sample was then baked at 180 ^{o}C and afterwards immersed in 3 M HCl at 80 ^{o}C to etch out Ni overnight. The free-standing GF was obtained by pyrolysis of the PMMA matrix at 800 ^{o}C for 15 min, and then washed with deionized water and air dried at room temperature. The mass of the ~20 mm x 20 mm x 1.6 mm GF product was about 20 mg. A previous attempt to remove the PMMA matrix by its dissolution in acetone was deemed unsuccessful. In that attempt, the composite was immersed in 20 mL acetone and heated to 80 °C and maintained at that temperature for 1 h. The sample was removed, washed with de-ionized water and air dried.

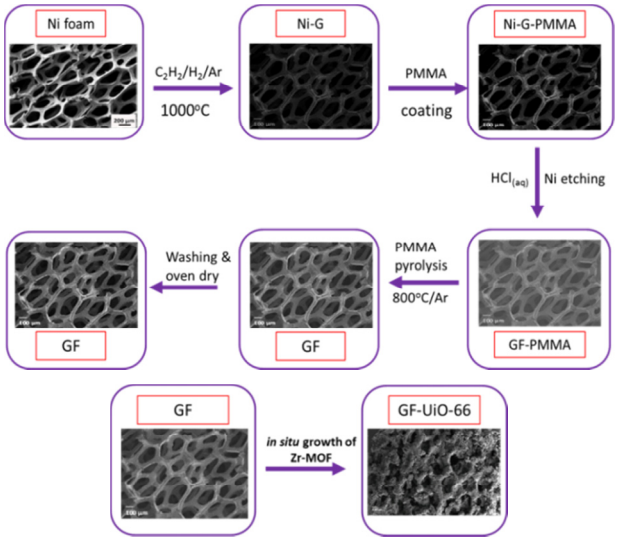

Fig. 1: General procedure for the synthesis of GF from Ni foam followed by *in-situ* MOF synthesis on GF surface.

2.4. *Preparation of GF/UiO-66 composites*

The preparation of GF/UiO-66 was carried out by an *in-situ* method whereby GF was placed in the synthesis mixture of UiO-66, which was derived following the steps described in section 2.2. It should be noted, however, that after the crystal growth the GF/UiO-66 samples were not centrifuged as this was found to destroy the 3D structure of the GF. Two approaches were undertaken: (i) Single-step growth which involved growing UiO-66 crystals directly from their precursors on the GF, and (ii) Two-step growth where the UiO-66 crystals were grown from their precursors in the first step and then in the second step, the resultant GF/UiO-66 was placed into a fresh reaction mixture and UiO-66 crystals grown on the composite surface.

2.5. Characterization

Powder X-ray diffraction (PXRD) patterns of pristine and composite materials were obtained using a Rigaku Ultima IV X-ray diffractometer with CBO technology using Ni-filtered Cu Kα radiation of 0.154 nm and a scanning speed of $5^{o}.s^{-1}$. The morphological analysis was carried out using an Auriga cobra Focused-Ion Beam Scanning Electron Microscope (FIB-SEM) where each sample was mounted on a carbon tape and coated with carbon (where necessary) prior to each analysis. Gas adsorption isotherm measurements were carried out on a Micromeritics ASAP 2020 HD instrument and all analyses were done at 77 K, with the hydrogen adsorption measured up to 1.2 bar of pressure. For each analysis the ultra-high purity grade (99.999 %) gas was used and each sample was degassed under vacuum (down to 10^{-7} bar) with heating up to 150 ^{o}C prior to each sorption isotherm measurement. The thermal stabilities were measured with a thermogravimetric analyzer (TGA) (Mettler, Toledo, TGA/SDTA 851e). For each run, 10 mg sample was heated to 1000 ^{o}C at a ramp rate of 10 $^{o}C.min^{-1}$ under 40 $mL.min^{-1}$ airflow. Using the laser confocal Raman microspectrometer (JY LabRam HR 800), the Raman spectra, structural and electronic features of the CVD-grown GF were obtained. The wavelength of the excitation laser used for all measurements was around 532 nm (~ 2.33 eV).

3. Results and discussion

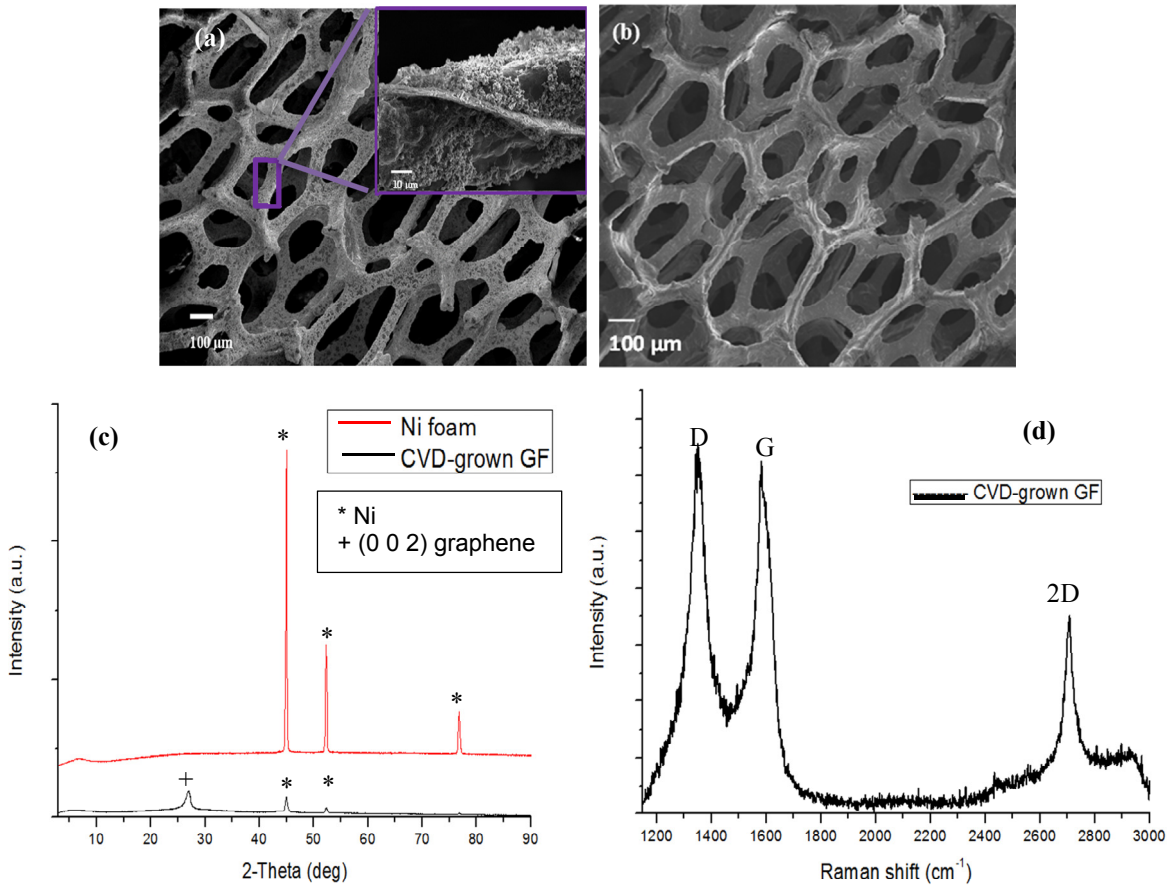

Fig. 2: (a) SEM image of CVD-grown GF obtained upon PMMA removal with acetone; (b) SEM image of GF obtained upon PMMA pyrolysis; (c) PXRD patterns of pristine Ni foam and Ni foam after CVD process; and (d) Raman spectrum for CVD product showing presence of graphene.

The SEM images of the GF obtained after the CVD process are presented in Figs. 2(a) and (b). It can be seen that after the removal of the PMMA polymer matrix using acetone, there was a significant amount of contaminants on the surface of the GF. This was most likely due to partial dissolution of PMMA in acetone and some of it remaining on the GF surface after the sample was dried. It was seen, however, that pyrolysis at 800 ^{o}C was more efficient at removing PMMA whereby the PMMA matrix was completely decomposed, leaving behind a GF surface with negligible surface contaminants. As shown in Fig. 2(c) the PXRD pattern obtained for pristine Ni foam was significantly different from that of the CVD product. A new diffraction peak around a 2-theta value of 27^{o} was observable and this indicated the presence of graphitic carbon after the CVD process. In Fig. 2(d), the product was shown to consist of the characteristic graphene D, G, and 2D Raman shift bands at approximately 1350, 1580 and 2700 cm^{-1}, respectively. The intensities of these bands can reveal some information about the type of graphene that was obtained, such as the presence of defects and number of graphene layers [18]. The calculated value for I_{2D}/I_G was ~0.6 which is representative of multi-layered graphene, and I_D/I_G of ~1.2 indicated a high level of defects in the graphene. Since the D band only occurs in graphene with Raman-active defects the I_D/I_G value is a measure of the extent of defects [19]. The results show successful synthesis of GF, which retained the structure of the Ni foam precursor after the CVD process. It is, however, important to note that not all the Ni was removed from the etching process as it can be seen in Fig. 2(c) that the Ni peaks at 45^{o} and 54^{o} were clearly observable. This was further confirmed by SEM-EDX mapping where it was found that about 10.6 % Ni was still present in the bulk carbon-containing product as shown in Fig. 3(a). The elemental maps further revealed that Ni was homogeneously distributed within the bulk carbon-containing product. It is not so undesirable for Ni to be present as it has also been shown in other studies to aid in H_2 uptake [20]. It is noteworthy that in the latter study hydrogen storage enhancement was reported at room temperature.

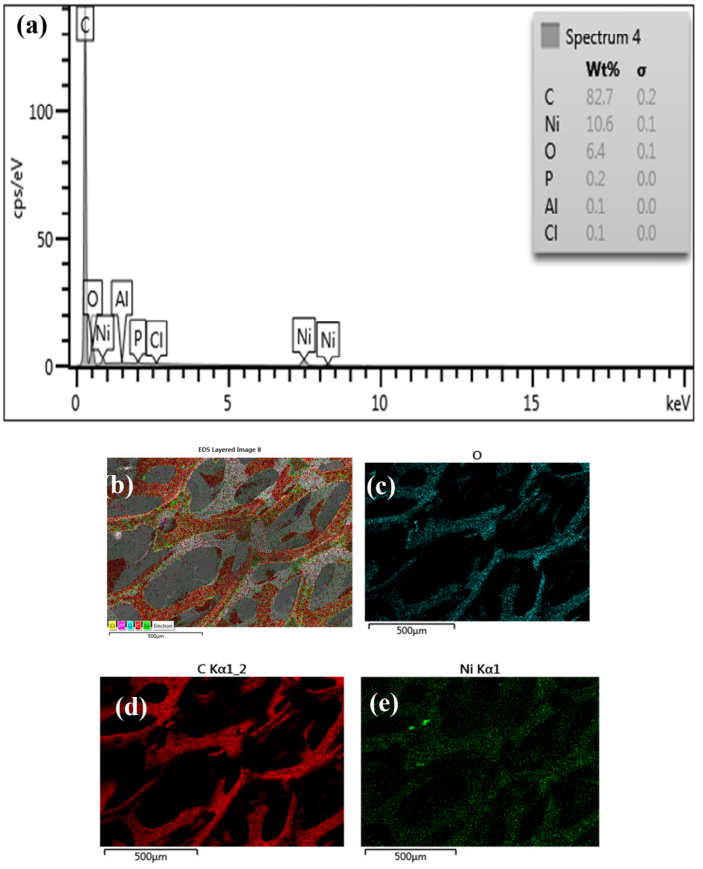

Fig. 3: (a) EDX spectrum of GF; (b) EDX layered image of GF, and (c) – (e) corresponding elemental maps for O, C, and Ni.

The use of a modulated synthesis approach for UiO-66 has been previously demonstrated to yield large crystals with good thermal and moisture stabilities [4,14]. As shown in Fig. 4(a) the method used in this study also gave similar large-sized UiO-66 crystals. However, it was found that for the *in-situ* synthesized MOF in the presence of GF, the average crystal size was significantly less than that obtained for pristine UiO-66 (Fig. 4(b)).

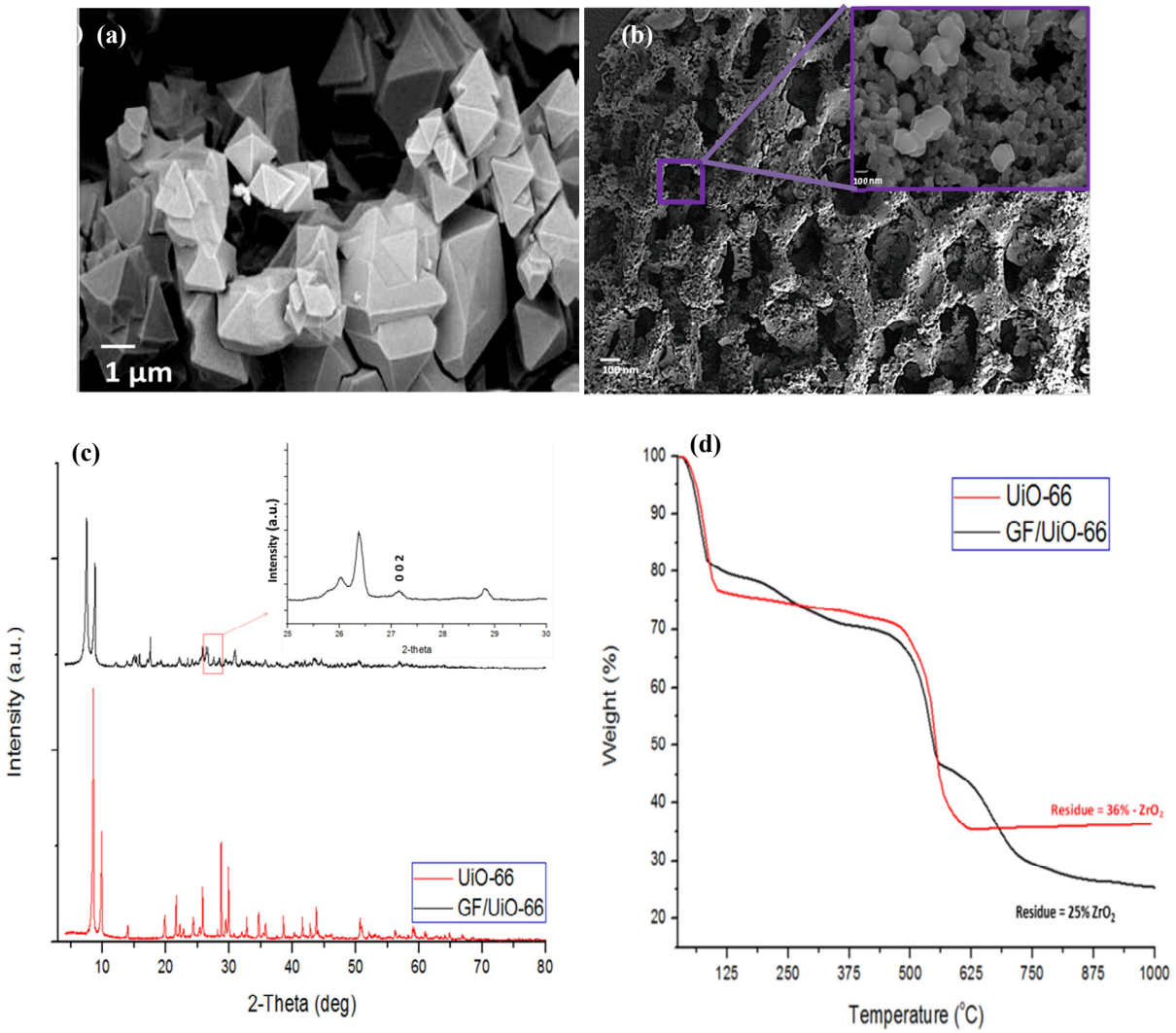

Fig. 4: (a) SEM image of pristine UiO-66; (b) SEM image of GF/UiO-66; (c) PXRD patterns for pristine UiO-66 and GF/UiO-66; and (d) TGA curves for pristine UiO-66 and GF/UiO-66 composite.

From similar studies conducted by Petit *et al.* [21] it was reported that functionalisation of graphene is important for compositing with MOFs. They showed that the absence or lack of functionalised groups on multi-layered structured graphene/graphite does allow for the growth of MOF crystals onto the surface but tend to disrupt the complete formation of the MOF, and thus generally leading to a distorted crystal being formed. The results were based on a different MOF, namely HKUST-1, which was prepared specifically with graphite and not CVD-grown graphene GF. Some of their observations, however, may also be true in this study. The PXRD patterns for pristine UiO-66 and GF/UiO-66 composite are presented in Fig. 4(c).

It can be seen that the growth of UiO-66 crystals was not inhibited in the presence of GF as the PXRD patterns of both pristine and GF/UiO-66 composite had very similar peak positions. The relative peak intensities were found to follow a similar trend with the addition of the (0 0 2) peak around 27° belonging to graphene in GF/UiO-66

composite. In Fig. 4(b) the insert gives an indication of the crystal shape and size at higher magnification and shows that the UiO-66 crystals tended to form agglomerates on the GF surface, which could indicate that they had less interactions with the graphene foam surface. Petit *et al.* [21] attributed such behaviour for a graphite/HKUST-1 sample to the lack of binding groups (e.g. oxygen groups) on the graphite surface which could facilitate the graphite/MOF interaction. These observations may be required to be investigated further at a later stage in this study as it was important to compare the gas adsorption properties (BET surface area and H_2 uptake) for UiO-66 crystals grown onto a GF surface using a single-step approach compared to a two-step *in-situ* synthesis method.

Fig. 4(d) presents the TGA curves for pristine UiO-66 and GF/UiO-66 composite. It can be seen from both thermograms that pristine UiO-66 and the GF/UiO-66 composite exhibited an initial weight loss from room temperature to about 100 ^{o}C as the samples were heated. This can be attributed largely to the removal of volatiles on the surface such as moisture or surface impurities. A further weight loss up to about 375 ^{o}C occurred for GF/UiO-66. This mass loss probably corresponds to the removal of all organic material, including sublimation and decomposition of residual terephthalic acid, and the evaporation of guest molecules from the pores such as solvent DMF. The second major weight loss step for both UiO-66 and GF/UiO-66 was found to occur around 550 ^{o}C which is attributed to the oxidative decomposition of the UiO-66 framework to form ZrO_2 [3,4]. It can also be seen that for the GF/UiO-66 composite, a third decomposition step was observed at 560 - 690 ^{o}C and this was due to the oxidation of carbon to carbon dioxide (CO_2). The residue yields for pristine UiO-66 and GF/UiO-66 were 36 and 25 wt%, respectively, which is expected as UiO-66 was a fraction of the GF/UiO-66 composite. The TGA results showed that the complete thermal decomposition of GF/UiO-66 occurred at a higher temperature compared to pristine UiO-66.

Table 1. BET surface area and hydrogen uptake for UiO-66 and GF/UiO-66 composites

Sample	BET S.A. ($m^2.g^{-1}$)	H_2 uptake at 77 K and 1.2 bar (wt%)
UiO-66	1367	1.5
GF/UiO-66 (single-step growth)	665	0.9
GF/UiO-66 (two-step growth)	1073	1.1

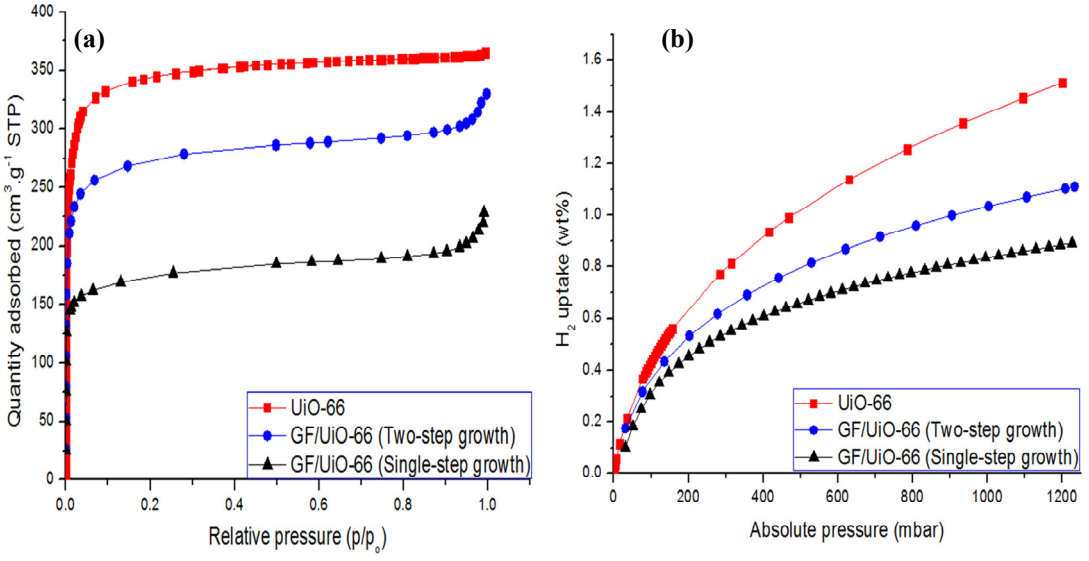

Fig. 5: (a) N_2 adsorption isotherm for BET surface area determination, and (b) H_2 uptake measured at 77 K and 1.2 bar pressure.

The sorption isotherm results in Table 1 and Fig. 5 show that both BET surface area and H_2 uptake for the composite GF/UiO-66 were less than the values for pristine UiO-66. Given that the UiO-66 crystals on the GF surface constitute a fraction of the composite itself, such a result can be expected. The results further demonstrate that using a two-step growth method led to a composite with enhanced BET surface area and H_2 uptake relative to the composite derived from a single-step growth method. Therefore, the two-step growth method was more effective, allowing more UiO-66 crystals to grow on the GF surface resulting in improved properties. These findings are in agreement with our previous study which demonstrated that an increase in the loading of MIL-101 crystals on Ni foam increased both the BET surface area and H_2 uptake capacity of the composite [22]. The results obtained in this study, therefore, show promise that the possible stepwise MOF crystal growth onto a GF surface, using *in-situ* solvothermal synthesis, could be undertaken to further improve the BET surface area and H_2 uptake capacity of a GF/MOF composite.

4. Conclusion

In this study, the preparation of GF/UiO-66 composites using *in-situ* solvothermal MOF synthesis was successful. It was further shown that the UiO-66 crystals could be grown onto the surface of GF using a two-step growth method, and compared to a single-step growth method, the former was found to give GF/UiO-66 composites with improved BET surface area and H_2 uptake capacity. The GF/UiO-66 composites were also shown to undergo complete thermal decomposition at a higher temperature than pristine UiO-66. These results show promise moving towards the system integration of MOFs for H_2 storage application purposes taking advantage of the superior thermal conductivity of graphene.

Acknowledgement

The authors would like to acknowledge financial support from the South African Department of Science and Technology (DST) towards HySA Infrastructure (Grant No. HTC004X). This work was also supported by the Royal Society – DFID Africa Capacity Building Initiative Programme Grant (Grant No. HTC070X).

References

[1] O.K. Farha, I. Eryazici, N.C. Jeong, B.G. Hauser, C.E. Wilmer, A.A. Sarjeant, R.Q. Snurr, S.T. Nguyen, A.O. Yazaydin, J.T. Hupp, J. Am. Chem. Soc. 134 (2012) 15016 – 15021.

[2] C. Wang, X. Liu, J.P. Chen, K. Li, Sci. Rep. 5: 16613 (2015) 1 - 10.

[3] J.H. Cavka, S. Jakolosen, U. Olsbye, N. Guillou, C. Lamberti, S. Bordiga, K.P. Lillerud, J. Am. Chem. Soc. 130 (2008) 13850 - 13851.

[4] J. Ren, T. Segakweng, H.W. Langmi, N.M Musyoka, B.C. North, M. Mathe, D. Bessarabov, Int. J. Mater. Res. 105 (2014) 516 - 519.

[5] B. Chen, N.W. Ockwig, A.R. Millward, D.S. Contreras, O.M. Yaghi, Angew. Chem. Int. 44 (2005) 4670 – 4679.

[6] G.W. Peterson, J.B. DeCoste, T.G. Glover, Y. Huang, H. Jasuja, K.S. Walton, Microporous Mesoporous Mater. 179 (2015) 48 – 53.

[7] N. Chanut, A.D. Wiersum, U-H. Le, Y.K. Hwang, F. Ragon, H. Chevreau, S. Bourrelly, B. Kuchta, J-S. Chang, C. Serre, L. Llewellyn, Eur. J. Inorg. Chem. (2016) 4416 – 4423.

[8] J. Ren, N.M. Musyoka, H.W. Langmi, A. Swartbooi, B.C. North, M. Mathe, Int. J. Hydrogen Energy 40 (2015) 4617 - 4622.

[9] D. Liu, J.J. Purewal, J. Yang, A. Sudik, S. Mauer, U. Mueller, J. Ni, D.J. Siegel, Int. J. Hydrogen Energy 37 (2012) 6109 – 6117.

[10] S. Yadav, Z. Zhu, C.V. Singh, Int. J. Hydrogen Energy 39 (2014) 4981 – 4995.

[11] A. Klechikov, G. Mercier, T. Sharifi, I.A. Baburin, G. Seifert, A.V. Yalyzin, Chem. Commun. 15 (2015) 15280 – 15283.

[12] H. Zhon, X. Liu, J. Zhang, X. Yan, Y. Liu, A. Yuan, Int. J. Hydrogen Energy 39 (2014) 2160 – 2167.

[13] Y.C. Yong, X.C. Dong, M.B. Chan-Park, H. Song, P. Chen, ACS Nano 6 (2012) 2394.

[14] J. Ren, H.W. Langmi, B.C. North, M. Mathe, D. Bessarabov, Int. J. Hydrogen Energy 39 (2014) 890 -895.

[15] Z. Chen, W. Ren, L. Gao, B. Liu, S. Pei, H-M. Cheng, Nat. Mater. 10 (2011) 424 – 428.

[16] S. Bhaviripudi, X. Jia, M.S. Dresselhaus, J. Kong, Nano Lett. 10 (2010) 4128 – 4133.

[17] S. Kumar, N. McEvoy, T. Lutz, G.P. Keeley, V. Nicolosi, C.P. Murray, W.J. Blau, G.S. Duesberg, Chem. Commun. 46 (2010) 1422 – 1424.

[18] R.S. Edwards, K.S. Coleman, Acc. Chem. Res. 46 (2013) 23 - 30.

[19] A.C. Ferrari, D.M. Basko, Nat. Nanotechnol. 8 (2013) 235−246.

[20] M. Zieliński, R. Wojcieszak, S. Monteverda, M. Mercy, M.M. Bettahar, Int. J. Hydrogen Energy 32 (2007) 1024 - 1032.

[21] C. Petit, B. Mendoza, D. O'Donnell, T.J. Bandos, Langmuir 27 (2011) 10234 – 10242.

[22] J. Ren, T. Segakweng, H.W. Langmi, B.C. North, M. Mathe, J. Alloys Comp. 645 (2015) S170–S173.